# Gradient Elastodamage Model for Quasi-Brittle Materials with an Evolving Internal Length

Antonios Triantafyllou[1]; Philip C. Perdikaris, M.ASCE[2]; and Antonios E. Giannakopoulos[3]

**Abstract:** The article presents a new approach based on a strain gradient damage constitutive law for modeling quasi-brittle materials such as concrete. The authors use a weak type nonlocal formulation of the problem, relying on Mindlin's Form II strain gradient elasticity theory. Gibbs free energy is used and the influence of the positive and negative principal strains to damage evolution is separated. Additional energy dissipation due to the gradient of the positive principal strains is introduced. The model requires an internal length, which is treated as an internal variable dependent on the level of damage. The study shows that the internal length increases with damage, corroborating available experimental results. Calibration of the gradient internal length evolution with damage is established through experimental data from two independent tests: a uniaxial tension or compression test to establish the evolution of damage, and a four-point bending (loading-unloading) test to relate the variation of the internal length with the accumulated level of damage. A numerical analysis of the response of a concrete beam specimen under four-point bending is presented to describe the calibration procedure. **DOI: 10.1061/(ASCE)EM.1943-7889.0000854.** 



## Introduction

This work aims to provide a new approach to a strain gradient damage constitutive law for modeling quasi-brittle materials and composites. Two reasons justify such an effort. Materials that exhibit strain softening are size sensitive (Bažant and Planas 1997) and their inelastic response manifesting itself through microcracking should be nonlocal (Bažant 1991). In other words, a length parameter is necessary not only for modeling any size effect present but also for ensuring that damage is not localized. A strain gradient theory can include such a length parameter and can address these issues in a physically consistent manner. Gradient theories can also address the issue of size effect in elasticity.

Elasticity and inelasticity for the case of softening materials are coupled by the very nature of the problem because damage is defined as a loss of the initial (elastic) stiffness due to material degradation. This work uses a weak type nonlocal formulation based on strain gradient elasticity and considers damage as a process affecting the gradient internal length.

The first issue addressed is whether the gradient internal length should evolve with damage. Several existing nonlocal damage theories assume a constant internal length (Pijaudier-Cabot and Bažant 1987; Mazars et al. 1991; Peerlings et al. 1996; Fremond and Nedjar 1996; de Borst and Gutierrez 1999; Comi 1999; Peerlings et al. 2001; Addessi et al. 2002; Benvenuti et al. 2002; Borino et al. 2003; Nguyen 2008; Poh and Swaddiwudhipong 2009; Desmorat et al. 2010) but there is strong evidence that this length is not constant. Geers et al. (1998) considered a finite-element formulation of a gradient damage model and concluded that an evolving internal length with an upper bound limit is necessary to predict a damage zone of a finite width. Pijaudier-Cabot et al. (2004) used acoustic emission experiments and micromechanical arguments to show that the internal length increases with damage starting from an initial value. Aggelis and Shiotani (2007, 2008) considered Rayleigh wave propagation in cementitious materials with thin inclusions simulating prescribed levels of damage, and found increasingly stronger dispersion of the Rayleigh waves with increasing damage. This, in the context of a gradient elastic damage model, can be explained by assuming an internal length increasing with damage (Georgiadis et al. 2004). Li (2011) and Li et al. (2011) arrived at the same conclusion using a homogenization procedure to derive a strain gradient constitutive law for the case of linear-elastic materials with microcracks. The present work uses a thermodynamic formulation to confirm this. However, it has been shown that, based on thermodynamics (Stamoulis and Giannakopoulos 2010) and experimental evidence on aluminum and nickel microbreams (Voyiadjis and Al-Rub 2005), this length should decrease with accumulated plastic strain. This is because of the inherent differences in the physics of gradient plasticity and damage theory (see Fig. 1).

Finally, selected experimental results on geometrical similar plain concrete beams subjected to four-point bending are presented and through a numerical example the calibration procedure of the gradient internal length evolution law is described. These experimental results are part of an extensive experimental program performed within the framework of this study, which is not the objective of the work presented here.

## Thermodynamic Formulation of the Problem

Mazars and Pijaudier-Cabot (1989), Murakami and Kamiya (1997), Wu et al. (2006) and many others proposed a thermodynamic formulation of a classical damage model based on the Helmholtz free energy. However, the present work follows the approach of Ortiz (1985), based on Gibbs energy (implying isothermal conditions). Ortiz's model for concrete was extended to include strain gradient effects by employing a simplified model with only one length parameter $g$, which is the simplest case of Mindlin's (1964) Form II strain gradient elasticity theory.

[1]Ph.D. Candidate, Dept. of Civil Engineering, Univ. of Thessaly, Volos 38334, Greece (corresponding author). E-mail: ant_triantafyllou@yahoo.gr

[2]Professor, Dept. of Civil Engineering, Univ. of Thessaly, Volos 38334, Greece.

[3]Professor, Dept. of Civil Engineering, Univ. of Thessaly, Volos 38334, Greece.

Note. This manuscript was submitted on May 11, 2014; approved on July 25, 2014; published online on September 8, 2014. Discussion period open until February 8, 2015; separate discussions must be submitted for individual papers. This paper is part of the ***Journal of Engineering Mechanics***, © ASCE, ISSN 0733-9399/04014139(13)/$25.00.

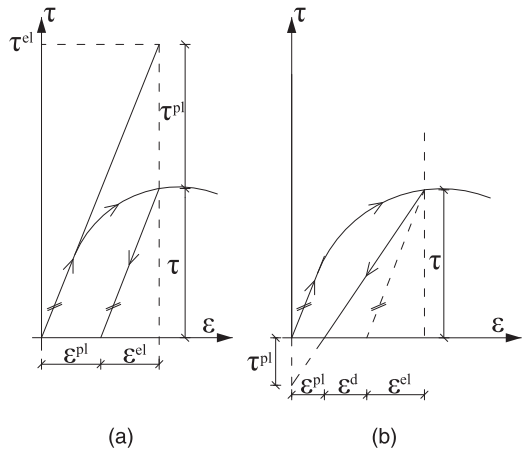


**Fig. 1.** Stress-strain diagram illustrating loading-unloading cycle for (a) plasticity and (b) damage; el = elastic; pl = plastic; d = damage

Gibbs energy density for the isothermal process within the framework of strain gradient elasticity in a Cartesian frame ($x_k$) is

$$G = \frac{1}{2}\boldsymbol{\tau} : \mathbf{C} : \boldsymbol{\tau} + \frac{1}{2}\boldsymbol{\lambda} \therefore \mathbf{B} : \boldsymbol{\lambda} - A^c \tag{1}$$

where $\boldsymbol{\tau}(\tau_{ij})$ = Cauchy stress; $\mathbf{C}(C_{ijkl})$ = fourth-order elasticity tensor; $\boldsymbol{\lambda}(\lambda_{ijk})$ = double-stress taken as $\boldsymbol{\lambda} = g^2\nabla\boldsymbol{\tau}(\lambda_{kij} = g^2\partial\tau_{ij}/\partial x_k)$; $\mathbf{B}$ = fourth-order tensor taken as $\mathbf{B} = (1/g^2)\mathbf{C}$; and $A^c$ = free energy density for microcrack formation. The symbols $(:)$ and $(\therefore)$ denote the two- and three-index product, respectively, i.e., $(B : \lambda)_{ijk} = B_{ijmn}\lambda_{kmn}$, $\boldsymbol{\lambda} \therefore \mathbf{B} : \boldsymbol{\lambda} = \lambda_{ijk}B_{ijmn}\lambda_{kmn}$, $(C : \tau)_{ij} = C_{ijkl}\tau_{kl}$, $\boldsymbol{\tau} : \mathbf{C} : \boldsymbol{\tau} = \tau_{ij}C_{ijkl}\tau_{kl}$ (repeated indexes imply summation from 1 to 3).

The stress-strain relations corresponding to Gibbs energy density [Eq. (1)] are given by $\boldsymbol{\varepsilon} = \partial G/\partial\boldsymbol{\tau} = \mathbf{C} : \boldsymbol{\tau} = \boldsymbol{\varepsilon}^e + \boldsymbol{\varepsilon}^i$ and $\boldsymbol{\kappa} = \partial G/\partial\boldsymbol{\lambda} = \mathbf{C} : \nabla\boldsymbol{\tau} = \nabla\boldsymbol{\varepsilon} = \nabla(\boldsymbol{\varepsilon}^e + \boldsymbol{\varepsilon}^i)$, where $\boldsymbol{\varepsilon}(\varepsilon_{ij})$ = infinitesimal strain tensor; and $\boldsymbol{\kappa} = \nabla\boldsymbol{\varepsilon}(\kappa_{kij} = \partial\varepsilon_{ij}/\partial x_k)$ = strain gradient third-order tensor. Also, the total stress is $\boldsymbol{\sigma} = \boldsymbol{\tau} - \nabla\boldsymbol{\lambda} = \boldsymbol{\tau} - g^2\nabla^2\boldsymbol{\tau}$. The equilibrium equations and the kinematic boundary conditions originating from the total stress expression can be found in Georgiadis and Grentzelou (2006).

The stress-strain time rate relations are given by: $\dot{\boldsymbol{\varepsilon}} = \mathbf{C} : \dot{\boldsymbol{\tau}} + \dot{\mathbf{C}} : \boldsymbol{\tau} = \dot{\boldsymbol{\varepsilon}}^e + \dot{\boldsymbol{\varepsilon}}^i$ and $\dot{\boldsymbol{\kappa}} = \nabla\dot{\boldsymbol{\varepsilon}}^e + \nabla\dot{\boldsymbol{\varepsilon}}^i = \dot{\boldsymbol{\kappa}}^e + \dot{\boldsymbol{\kappa}}^i$, where $\dot{(\cdot)} = \partial/\partial t$ and the superscripts $e$ and $i$ denote the elastic and inelastic rate of deformation due to degradation of the elastic material properties, respectively.

Microcracking can be physically viewed as added flexibility to the initial flexibility of an uncracked material. Following Ortiz (1985), the elastic compliance tensor is taken as a characterization of the state of material damage. Therefore, the elastic compliance can be described by an additive formulation

$$\mathbf{C} = \mathbf{C}^0 + \mathbf{C}^c \tag{2}$$

where $\mathbf{C}^0$ = elasticity tensor of the uncracked material initially assumed as isotropic; and $\mathbf{C}^c$ = added flexibility due to microcrack opening under the current applied stress field.

In essence, the inelastic flexibility is the sum of the initial plus the additional flexibility due to the presence of distributed microcracking in the material, which is justifiable in terms of the softening and is in line with self-consistent calculations of the overall elastic compliance of elastic media with distributed cracking (Budiansky and O'Connell 1976; Kachanov 1980; Horii and Nemat-Nasser 1983). Hence, the total strain and strain gradient due to cracking can be written as

$$\begin{aligned} \boldsymbol{\varepsilon} &= \left(\mathbf{C}^0 + \mathbf{C}^c\right) : \boldsymbol{\tau} = \boldsymbol{\varepsilon}^0 + \boldsymbol{\varepsilon}^c \\ \boldsymbol{\kappa} &= \nabla\boldsymbol{\varepsilon}^0 + \nabla\boldsymbol{\varepsilon}^c = \boldsymbol{\kappa}^0 + \boldsymbol{\kappa}^c \end{aligned} \tag{3}$$

### Opening and Closing of Microcracks

Cracks in concrete, as well as in other quasi-brittle materials, can develop even under compressive stress conditions. Also, opened cracks can at some point close and not propagate. The closing of cracks and the resulting stiffening of the material explains the characteristic S-shaped hysteretic loops that are observed experimentally in flexural members subjected to cyclic loading.

To mathematically model opening or closing microcracks, the positive and negative orthogonal projections $\mathbf{P}^+$ and $\mathbf{P}^-$ of the strain space onto the positive and negative cones $C^+$ and $C^-$ are introduced. This operator assigns to every state of strain $\boldsymbol{\varepsilon}$ its point $\mathbf{P}^+\boldsymbol{\varepsilon}$ and $\mathbf{P}^-\boldsymbol{\varepsilon}$ on $C^+$ and $C^-$, respectively. If $\varepsilon^{(a)}$ and $d^{(a)}$ $(a = 1, 2, 3)$ denote the eigenvalues and eigenvectors of the total strain $\boldsymbol{\varepsilon}$, respectively, so that $\varepsilon_{ij} = \sum_{a=1}^{3}\varepsilon^{(a)}d_i^{(a)}d_j^{(a)}$, then the positive projection of $\boldsymbol{\varepsilon}$ is given by $(P^+\boldsymbol{\varepsilon})_{ij} = \varepsilon_{ij}^+ = \sum_{a=1}^{3}\langle\varepsilon^{(a)}\rangle d_i^{(a)}d_j^{(a)}$, where $\langle x\rangle = (x + |x|)/2$ is the Macauley bracket, and the negative projection is $\mathbf{P}^- = \mathbf{I} - \mathbf{P}^+$ ($\mathbf{I}$ = identity tensor).

For a given state of stress $\boldsymbol{\tau}$ consistent with the closing mode of microcracks, the following minimization problem must be satisfied:

$$\text{minimize} : \frac{1}{2}\boldsymbol{\varepsilon} : \left(\mathbf{C}^0 + \overline{\mathbf{C}}^c\right)^{-1} : \boldsymbol{\varepsilon} - \boldsymbol{\tau} : \boldsymbol{\varepsilon} \text{ subject to} : \varepsilon^{c(a)} \geq 0 \tag{4}$$

where $\overline{\mathbf{C}}^c$ is the added flexibility due to the opening of all microcracks and $\varepsilon^{c(a)}$ are the eigenvalues of the inelastic strain, $\boldsymbol{\varepsilon}^c = \boldsymbol{\varepsilon} - \mathbf{C}^0 : \boldsymbol{\tau}$.

For a given state of stress gradient $\nabla\boldsymbol{\tau}$, the minimization problem is

$$\text{minimize} : \frac{1}{2}\nabla\boldsymbol{\varepsilon} \therefore \left(\mathbf{C}^0 + \overline{\mathbf{C}}^c\right)^{-1} : \nabla\boldsymbol{\varepsilon} - \nabla\boldsymbol{\tau} \therefore \nabla\boldsymbol{\varepsilon} \text{ subject to} : \nabla\varepsilon^{c(a)} \geq 0 \tag{5}$$

The solution to Eqs. (4) and (5) can be approximated, respectively as

$$\boldsymbol{\varepsilon} \approx \mathbf{C}^0 : \boldsymbol{\tau} + \mathbf{P}^+\left(\overline{\mathbf{C}}^c : \boldsymbol{\tau}^+\right) \tag{6a}$$

and

$$\nabla\boldsymbol{\varepsilon} \approx \mathbf{C}^0 : \nabla\boldsymbol{\tau} + \mathbf{P}^+\left[\overline{\mathbf{C}}^c : (\nabla\boldsymbol{\tau})^+\right] \tag{6b}$$

where $\tau_{ij}^+ = P^+(\tau_{ij}) = \sum_{a=1}^{3}\langle\tau^{(a)}\rangle q_i^{(a)}q_j^{(a)}$; $\tau^{(a)}$ and $\mathbf{q}^{(a)}$ = eigenvalues and eigenvectors of $\boldsymbol{\tau}$; and $(\nabla\tau)_{ijk}^+ \approx \sum_{a=1}^{3}(\partial\langle\tau^{(a)}\rangle/\partial x_i)^+ q_j^{(a)}q_k^{(a)}$ [for Eq. (6a), see Ortiz 1985].

For the stress-strain relations to be consistent with Eq. (6), it must be true that $\boldsymbol{\varepsilon}^c = \mathbf{C}^c : \boldsymbol{\tau} = \mathbf{P}^+(\overline{\mathbf{C}}^c : \boldsymbol{\tau}^+)$ and $\nabla\boldsymbol{\varepsilon}^c = \mathbf{C}^c : \nabla\boldsymbol{\tau} = \mathbf{P}^+(\overline{\mathbf{C}}^c : (\nabla\boldsymbol{\tau})^+)$. Finally, the added flexibility tensor due to the opening of microcracks can be approximated as

$$\mathbf{C}^c = \mathbf{P}^+ : \overline{\mathbf{C}}^c : \mathbf{P}^+ \quad \left(C_{ijkl}^c = P_{ijmn}^+\overline{C}_{mnpq}^c P_{pqkl}^+\right) \tag{7}$$

Recalling that $\boldsymbol{\varepsilon}^c = \mathbf{C}^c : \boldsymbol{\tau}$, the positive and negative strain projections based on the positive and negative stress projections can be approximated as $\mathbf{P}^+(\boldsymbol{\varepsilon}^c) = \mathbf{P}^+[\overline{\mathbf{C}}^c : \mathbf{P}^+(\boldsymbol{\tau})] = \mathbf{P}^+(\overline{\mathbf{C}}^c : \boldsymbol{\tau}^+)$ and $\mathbf{P}^-(\boldsymbol{\varepsilon}^c) = \mathbf{P}^-(\overline{\mathbf{C}}^c : \boldsymbol{\tau}^-)$, respectively.

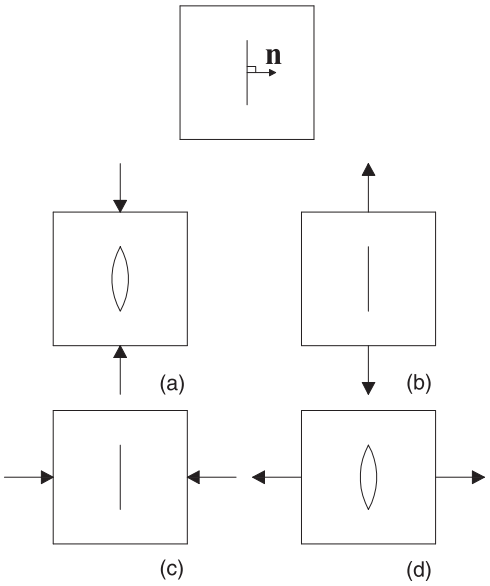


**Fig. 2.** State of microcracks: (a and d) opening mode; (b and c) closing mode [Reprinted from *Mechanics of Materials*, Vol. 4, M. Ortiz, "A constitutive theory for the inelastic behavior of concrete," 67–93, Copyright (1985) with permission from Elsevier]

To further illustrate the necessity of the previous mathematical manipulations, a microcrack normal to a unit vector $\mathbf{n}$ is considered. Any stress acting upon a planar microcrack can be analyzed in any of the four possible loading configurations depicted in Fig. 2. The cases in Figs. 2(b and d) refer to nonzero positive projections ($\boldsymbol{\tau} = \boldsymbol{\tau}^+$) whereas the cases in Figs. 2(a and c) refer to nonzero negative projections ($\boldsymbol{\tau} = \boldsymbol{\tau}^-$). The orientation of the stress in Figs. 2(b and c) is normal to the crack plane; that is, $\mathbf{n} \cdot \boldsymbol{\tau}^+ \cdot \mathbf{n} = 0$ and $\mathbf{n} \cdot \boldsymbol{\tau}^- \cdot \mathbf{n} = 0$, respectively, preventing crack propagation. Therefore, microcrack opening occurs due to a tensile stress in Fig. 2(d) and a compressive one in Fig. 2(a). These two cases correspond to a tensile and a compressive opening mode $I_T$ and $I_C$, respectively. Thus, the added flexibility tensor due to microcrack opening can be decomposed as $\overline{\mathbf{C}}^c = \overline{\mathbf{C}}^c_{I_T} + \overline{\mathbf{C}}^c_{I_C}$, and the inelastic deformation due to microcracking can be expressed as $\boldsymbol{\varepsilon}^c = \boldsymbol{\varepsilon}^c_{I_T} + \boldsymbol{\varepsilon}^c_{I_C}$. Microcrack opening under modes $I_T$ and $I_C$ implies that $\boldsymbol{\varepsilon}^c_{I_T} \geq 0$ and $\boldsymbol{\varepsilon}^c_{I_C} \leq 0$, respectively.

Summarizing, Gibbs energy becomes

$$G = \frac{1}{2}\boldsymbol{\tau} : \mathbf{C}^0 : \boldsymbol{\tau} + \frac{1}{2}\boldsymbol{\tau}^+ : \overline{\mathbf{C}}^c_{I_T} : \boldsymbol{\tau}^+ + \frac{1}{2}\boldsymbol{\tau}^- : \overline{\mathbf{C}}^c_{I_C} : \boldsymbol{\tau}^- + \frac{1}{2}g^2 \nabla\boldsymbol{\tau} \therefore \mathbf{C}^0 : \nabla\boldsymbol{\tau} + \frac{1}{2}g^2 (\nabla\boldsymbol{\tau})^+ \therefore \overline{\mathbf{C}}^c_{I_T} : (\nabla\boldsymbol{\tau})^+ - A^c \quad (8)$$

It is true that the stress gradient in Eq. (8) induces only mode $I_T$ crack opening because there are no terms of the type $(\nabla\boldsymbol{\tau})^-$. This is further clarified in Appendix I.

### Damage Rules

The evolution of the tensorial damage parameter $\mathbf{C}^c$[Eq. (2)] can be described based on the evolution of $\overline{\mathbf{C}}^c$ according to a damage rule of the general form $\overline{\mathbf{C}}^c = \overline{\mathbf{C}}^c_{I_T} + \overline{\mathbf{C}}^c_{I_C}$ (Ortiz 1985) with

$$\dot{\overline{\mathbf{C}}}^c_{I_T} = \dot{\mu}\mathbf{R}_{I_T}(\boldsymbol{\tau}) \quad \text{and} \quad \dot{\overline{\mathbf{C}}}^c_{I_C} = \dot{\mu}\mathbf{R}_{I_C}(\boldsymbol{\tau}) \quad (9)$$

where $\mathbf{R}_{I_T}(\boldsymbol{\tau})$, $\mathbf{R}_{I_C}(\boldsymbol{\tau})$ = material response functions (fourth-order dimensionless tensors) that determine the direction in which damage should occur; and $\mu$ = internal scalar parameter (dimensions area/force), which may be regarded as a measure of the cumulative damage resulting in a decrease of the unloading elastic modulus. In plasticity theory, the parameter $\mu$ resembles the accumulated equivalent plastic strain. A localization analysis for the case of uniaxial tension is included in Appendix I, where it is shown that the proposed nonlocal model leads to objective and mesh-independent results if used in a FEM analysis.

Initially, the material is assumed to be uncracked ($\mu = 0$) and initial conditions reign. The proposed damage rules presented include only the Cauchy (local) part of the total stress. The proposed model will be calibrated through experimental strain data and hence the damage rules will be associated with the energetically conjugate quantity of strain; that is, the Cauchy part of the total stress. It should be emphasized that this assumption has a physical justification because the damage surface of a quasi-brittle material is established through experimental results of uniaxial tests and in the case of uniform loading there in no gradient effect. The choice of local stress in Eq. (9) can be further justified from the work of Simone et al. (2004) who showed that the use of a nonlocal dissipation-driving state variable (i.e., the total stress or total strain of the gradient formulation) leads to an incorrect failure characterization in terms of damage initiation and propagation ahead of a macrocrack. The proposed approach uses the inelastic strains for the tensorial characterization of damage. Bui (2010) used a similar approach, introducing a mixed (local and nonlocal) formulation for damage characterization.

The irreversible character of damage necessitates that $\dot{\mu} \geq 0$. The condition $\dot{\mu} > 0$ refers to active damage mechanisms, whereas $\dot{\mu} = 0$ refers to elastic behavior. Therefore, $\mathbf{R}_{I_T}(\tau)$ and $\mathbf{R}_{I_C}(\tau)$ must be positive definite. Furthermore, the internal length of the material, $g$, is assumed to be a function of the damage level [that is, $g = g(\mu)$], and the rate of change of the internal length is $\dot{g} = \dot{\mu}(dg/d\mu)$.

It should be emphasized that the present work is based on gradient elasticity, whereas inelasticity (damage) is treated as a process affecting the parameters of gradient elasticity, the internal length, and the classical elastic properties (Rodriguez-Ferran et al. 2011). In this thermodynamic formulation, there are two internal variables, the damage parameter, $\mu$, and the internal length, $g$, with a constraint demand for the internal length to be a function of the damage parameter. Based on these assumptions, the energy density dissipation [see Eq. (1)] inequality can be expressed as

$$d = \frac{1}{2}\boldsymbol{\tau} : \dot{\overline{\mathbf{C}}}^c : \boldsymbol{\tau} + \frac{1}{2}g^2 \nabla\boldsymbol{\tau} \therefore \dot{\overline{\mathbf{C}}}^c : \nabla\boldsymbol{\tau} + \frac{1}{2}\dot{(g^2)}\ (\nabla\boldsymbol{\tau})^+ \therefore \overline{\mathbf{C}}^c : (\nabla\boldsymbol{\tau})^+ - \dot{A}^c \geq 0 \quad (10)$$

where $d$ signifies the rate of energy dissipation density.

Substituting Eq. (9) into Eq. (10), the rate of energy dissipation becomes

$$d = \left[\frac{1}{2}\boldsymbol{\tau}^+ : \mathbf{R}_{I_T} : \boldsymbol{\tau}^+ + \frac{1}{2}\boldsymbol{\tau}^- : \mathbf{R}_{I_C} : \boldsymbol{\tau}^- + \frac{1}{2}g^2 (\nabla\boldsymbol{\tau})^+ \therefore \mathbf{R}_{I_T} : (\nabla\boldsymbol{\tau})^+ + g\frac{dg}{d\mu}(\nabla\boldsymbol{\tau})^+ \therefore \overline{\mathbf{C}}^c : (\nabla\boldsymbol{\tau})^+\right]\dot{\mu} - \dot{A}^c \geq 0 \quad (11)$$

The rate of energy dissipation should be positive according to the second law of thermodynamics. Because $\mathbf{R}_{I_T}$, $\mathbf{R}_{I_C}$, $\mathbf{C}^c_{I_T}$, and $\mathbf{C}^c_{I_C}$ are positive definite and $\dot{\mu} \geq 0$, it follows that

$$dg/d\mu \geq 0 \quad (12)$$

Eq. (12) shows that if the internal length is allowed to evolve with damage, it must increase or remain constant with increasing damage.

The inelastic free energy density, $A^c$, associated with microcrack formation is a function of $\mu$. The rate of the free energy coincides

with the energy release rate per unit length of microcrack. Using a micromechanical model of fracture as a justification (see Appendix II for diluted microcracking), the rate of the inelastic free energy is defined as

$$\dot{A}^c = \dot{\mu}\frac{dA^c}{d\mu} = \left\{\frac{\pi}{2}t(\mu)^2 + \frac{1}{3}\left[\frac{\partial t(\mu)}{\partial \omega}\xi(\mu)\right]^2\right\}\dot{\mu} \tag{13}$$

where $t(\mu)$ = critical stress for damage extension; and $\omega$ = direction normal to the critical stress (along the microcrack). Note that $\xi(\mu)$ is half the microcrack length and Eq. (13) requires two tests: a uniaxial test $[\partial t(\mu)/\partial\omega = 0]$ to establish $t(\mu)$ and a pure bending test to establish $\partial t(\mu)/\partial\omega$.

Substituting Eq. (13) into Eq. (12) yields

$$d = \left\{\frac{1}{2}\boldsymbol{\tau}^+ : \mathbf{R}_{I_T} : \boldsymbol{\tau}^+ + \frac{1}{2}\boldsymbol{\tau}^- : \mathbf{R}_{I_C} : \boldsymbol{\tau}^- - \frac{\pi}{2}t(\mu)^2 + \frac{1}{2}g^2(\nabla\boldsymbol{\tau})^+ \therefore \mathbf{R}_{I_T} : (\nabla\boldsymbol{\tau})^+ + g\frac{dg}{d\mu}(\nabla\boldsymbol{\tau})^+ \therefore \overline{\mathbf{C}}^c : (\nabla\boldsymbol{\tau})^+ - \frac{1}{3}\left[\frac{\partial t(\mu)}{\partial\omega}\xi(\mu)\right]^2\right\}\dot{\mu} \geq 0 \tag{14}$$

Because $\dot{\mu} \geq 0$, Eq. (14) necessitates

$$\frac{1}{2}\boldsymbol{\tau}^+ : \mathbf{R}_{I_T} : \boldsymbol{\tau}^+ + \frac{1}{2}\boldsymbol{\tau}^- : \mathbf{R}_{I_C} : \boldsymbol{\tau}^- - \frac{\pi}{2}t(\mu)^2 \geq 0 \tag{15a}$$

and

$$\frac{1}{2}g^2(\nabla\boldsymbol{\tau})^+ \therefore \mathbf{R}_{I_T} : (\nabla\boldsymbol{\tau})^+ + g\frac{dg}{d\mu}(\nabla\boldsymbol{\tau})^+ \therefore \overline{\mathbf{C}}^c : (\nabla\boldsymbol{\tau})^+ - \frac{1}{3}\left[\frac{\partial t(\mu)}{\partial\omega}\xi(\mu)\right]^2 \geq 0 \tag{15b}$$

In Eqs. (15*a*) and (15*b*), the effects of stress gradient and damage, which influence the inelastic response, can be treated separately. Eq. (15*a*) corresponds to the case of $g = 0$ and Eq. (15*b*) addresses the influence of the internal length, $g$, and consequently of the stress gradient. In the absence of the stress gradient effect in Gibbs energy, Ortiz's model (1985) is recovered by Eq. (15*a*).

Next, a stress function $F$ is defined in the form

$$F(\boldsymbol{\tau}) = \frac{1}{2}\boldsymbol{\tau}^+ : \mathbf{R}_{I_T} : \boldsymbol{\tau}^+ + \frac{1}{2}\boldsymbol{\tau}^- : \mathbf{R}_{I_C} : \boldsymbol{\tau}^- = F_{I_T} + F_{I_C} \tag{16}$$

Substituting Eq. (16) into Eq. (15*a*), a damage function $\Phi$ is obtained as

$$\Phi(\boldsymbol{\tau}, \mu) = F(\boldsymbol{\tau}) - \frac{\pi}{2}t(\mu)^2 \geq 0 \tag{17}$$

and if the inequality in Eq. (17) is not satisfied, the material must behave elastically. For further damage to occur, the equality in Eq. (17) must be satisfied (see Fig. 3). Therefore, $F(\boldsymbol{\tau}) = (\pi/2)t(\mu)^2$ defines the elastodamage boundary in the local stress space. Thus, the onset of damage is characterized by the following criteria:

$$\Phi(\boldsymbol{\tau}, \mu) = F(\boldsymbol{\tau}) - \frac{\pi}{2}t(\mu)^2 = 0 \quad \text{and} \quad (\partial\Phi/\partial\boldsymbol{\tau}) : \dot{\boldsymbol{\tau}} = (\partial F/\partial\boldsymbol{\tau}) : \dot{\boldsymbol{\tau}} > 0 \tag{18}$$

These relations imply that for further damage the stress point must lie on the current damage surface and the stress increment must point outward of the elastic domain. A stress point inside the current damage surface will imply gradient elasticity.

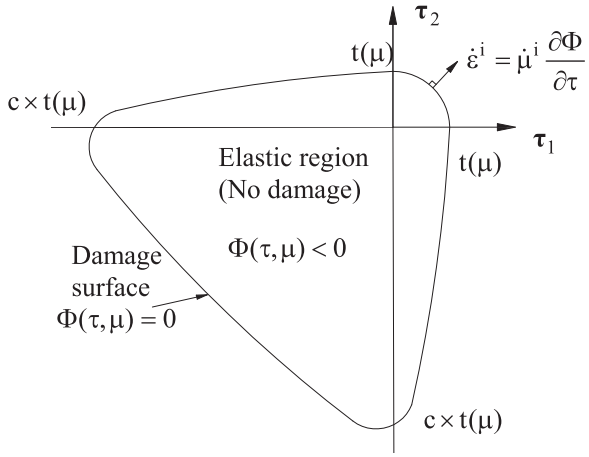


**Fig. 3.** Damage surface and damage criterion in local principal stress space

### *Associated Damage Rule*

The damage rule is associated if the following relations hold true for the damage direction tensors:

$$\mathbf{R}_{I_T} = \frac{\partial F_{I_T}}{\partial\boldsymbol{\tau}^+\partial\boldsymbol{\tau}^+} \quad \text{and} \quad \mathbf{R}_{I_C} = \frac{\partial F_{I_C}}{\partial\boldsymbol{\tau}^-\partial\boldsymbol{\tau}^-} \tag{19}$$

This assumption reduces the calibration to the determination of the scalar functions $F$ rather than the tensorial quantities $\mathbf{R}_{I_T}$ and $\mathbf{R}_{I_C}$. Furthermore, the inelastic strain rate tensor due to damage is

$$\dot{\boldsymbol{\varepsilon}}^i = \dot{\mathbf{C}} : \boldsymbol{\tau} = \dot{\mathbf{C}}^c : \boldsymbol{\tau} = \left(\mathbf{P}^+ : \ddot{\overline{\mathbf{C}}}^c : \mathbf{P}^+\right) : \boldsymbol{\tau} = \dot{\mu}\left(\mathbf{R}_{I_T} : \boldsymbol{\tau}^+ + \mathbf{R}_{I_C} : \boldsymbol{\tau}^-\right) \tag{20}$$

which, using Eq. (19), can be written as

$$\dot{\boldsymbol{\varepsilon}}^i = \dot{\mu}\left(\frac{\partial F_{I_T}}{\partial\boldsymbol{\tau}^+} + \frac{\partial F_{I_C}}{\partial\boldsymbol{\tau}^-}\right) = \dot{\mu}\partial F/\partial\boldsymbol{\tau} = \dot{\mu}\partial\Phi/\partial\boldsymbol{\tau} \tag{21}$$

Eq. (21) implies that the inelastic part of the strain rate tensor points outward and in a normal direction to the damage surface (see Fig. 3). In the context of a rate independent damage formulation, as suggested by Ortiz (1985)

$$\mathbf{R}_{I_T} = \frac{\boldsymbol{\tau}^+ \otimes \boldsymbol{\tau}^+}{(\boldsymbol{\tau}^+ : \boldsymbol{\tau}^+)} \quad \text{and} \quad \mathbf{R}_{I_C} = c\frac{\boldsymbol{\tau}^- \otimes \boldsymbol{\tau}^-}{(\boldsymbol{\tau}^- : \boldsymbol{\tau}^-)} \tag{22}$$

where $c$ = cross-effect coefficient governing the level of damage under compression ($c = 0$ for no cross-effect); $(\tau \otimes \tau)_{ijkl} = \tau_{ij}\tau_{kl}$ = dyadic product tensor; and $(\boldsymbol{\tau} : \boldsymbol{\tau}) = \tau_{ij}\tau_{ij}$ = trace of the $(\boldsymbol{\tau} \otimes \boldsymbol{\tau})$ tensor. The value of the critical stress $t(\mu)$ and the cross-effect coefficient, $c$, can be determined from uniaxial test results. Then, the damage surface simplifies to

$$\Phi = \frac{1}{2}\boldsymbol{\tau}^+ : \boldsymbol{\tau}^+ + \frac{1}{2}c\boldsymbol{\tau}^- : \boldsymbol{\tau}^- - \frac{\pi}{2}t^2(\mu) \tag{23}$$

It is worth noting that in this approach, because the effect of microcracking is directly linked with the elasticity tensor, an initially

isotropic material would become anisotropic with damage. In the case of nonassociative damage evolution and/or initially anisotropic elastic behavior, as observed in rocks, microcracking may not occur along the principal stress trajectories but localizes along specific weak surfaces in the material (Chen et al. 2012). Any existing directionality of microcrack opening, can be included in the response functions $\mathbf{R}_{I_T}$ and $\mathbf{R}_{I_C}$.

## Application to Plain Concrete

The proposed model is applied to plain concrete beams subjected to four-point bending, with damage occurring in the middle part of the beam subjected to pure bending, where axial normal stresses are principal and a uniaxial law for the concrete is assumed to be sufficient for damage characterization.

### Uniaxial Response

The uniaxial response of plain concrete under tension or compression is assumed to be of the form

$$\begin{aligned} &\tau_i = E_{0i}\varepsilon_i \quad \text{for} \quad \varepsilon_i \le \varepsilon_{0i} \quad \text{and} \\ &\tau_i = (1-D_i)E_{0i}\varepsilon_i = \frac{E_{0i}\varepsilon_i}{1+E_{0i}\mu_i} \quad \text{for} \quad \varepsilon_i > \varepsilon_{0i} \end{aligned} \tag{24}$$

where $E_{0i}$ = Young's modulus of elasticity of the uncracked material; $\varepsilon_{0i}$ = strain value depicting the end of a perfectly elastic response and initiation of damage; and $D_i$ (dimensionless), $\mu_i$ (stress$^{-1}$) = two equivalent damage parameters. The index $i = c, t$ is a subscript denoting compression or tension, respectively.

In a thermodynamic formulation, $\mu$ is used to avoid imposing the additional constraint $D \le 1$. However, both damage parameters can be used, given that

$$D = 1 - \frac{1}{1+E_0\mu} \tag{25}$$

It is obvious from Eq. (25) that if $\mu = 0$, then $D = 0$; and if $\mu \to \infty$, then $D \to 1$. In other words, both $\mu$ and $D$ describe the initiation and the evolution of damage in the same way; however, the limit for complete damage is bounded in the case of $D$, but this is not true for $\mu$. There is a one-to-one correspondence between $D$ and $\mu$ and $dD/d\mu|_{\mu=0} = E_0$.

If for the stress-strain response of plain concrete a relationship of the following form is assumed (Popovics 1973):

$$\tau_i = f_i \frac{\beta_i(\varepsilon/\varepsilon_i)}{\beta_i - 1 + (\varepsilon/\varepsilon_i)^{\beta_i}} \tag{26}$$

where $f_i$ = maximum stress; $\varepsilon_i$ = strain at maximum stress; and $\beta_i$ = material parameter that defines the steepness of the softening branch, a damage law for compression ($i = c$) and tension ($i = t$) can be derived based on Eqs. (24) and (26)

$$\begin{aligned} &D_i = 0 \quad \text{for} \quad \varepsilon < \varepsilon_{0i} \quad \text{and} \\ &D_i = 1 - \frac{\beta_i - 1 + (\varepsilon_{0i}/\varepsilon_i)^{\beta_i}}{\beta_i - 1 + (\varepsilon/\varepsilon_i)^{\beta_i}} \quad \text{for} \quad \varepsilon \ge \varepsilon_{0i} \end{aligned} \tag{27}$$

where the Young's modulus, $E_{0i}$, is equal to

$$E_{0i} = \frac{\beta_i f_i}{\left[\beta_i - 1 + (\varepsilon_{0i}/\varepsilon_i)^{\beta_i}\right]\varepsilon_i} \tag{28}$$

The threshold strain values for uniaxial tension, $\varepsilon_{0t}$, and for uniaxial compression, $\varepsilon_{0c}$, are assumed to occur at a stress $\tau_t = 0.8 f_t$ (Li and Li 2000) and $\tau_c = 0.4 f_c$, respectively. Therefore, the critical strain, $\varepsilon_{0i}$, signifying the onset of damage, can be determined using Eq. (26). Furthermore, assuming that the Young's modulus is the same in uniaxial tension and compression, an estimate for the tensile to compressive strain ratio at the peak stress is obtained as follows:

$$\frac{\varepsilon_t}{\varepsilon_c} = \frac{\beta_t f_t \left[\beta_c - 1 + (\varepsilon_{0c}/\varepsilon_c)^{\beta_c}\right]}{\beta_c f_c \left[\beta_t - 1 + (\varepsilon_{0t}/\varepsilon_t)^{\beta_t}\right]} \tag{29}$$

### Flexural Response

The local normal longitudinal strains in the part of the concrete beam specimens under pure bending are assumed to be linearly distributed along the depth of the beam's cross section ($z$-axis), $\varepsilon_{xx} = \varepsilon_m + kz$, where $\varepsilon_m$ = strain at $z = 0$, and $k$ = curvature. In the elastic region of the beam, $\varepsilon_m = 0$, and beyond the elastic limit the neutral axis shifts upward ($\varepsilon_m \neq 0$).

For a given value of $k$, and using the assumed law for uniaxial tension and compression, the value of $\varepsilon_m$ that satisfies equilibrium is determined through an iteration procedure. This implies a one-dimensional (1D) discretization of the cross section to strips of depth $dz$ to evaluate numerically the integral, $N = b\int_{-h/2}^{h/2} \sigma_{xx} dz = 0$. Essentially, in the proposed model, the input parameter is the curvature at midspan and the output is the bending moment capacity, $M = b\int_{-h/2}^{h/2} \sigma_{xx} z dz$, corresponding to the assumed linear axial strain distribution along the height of the cross section. The number of strips used to discretize the cross-sectional area is chosen based on a convergence requirement of a mesh refinement so that when the number of strips is doubled, there is a change of less than $10^{-5}$ kNm in the predicted value of $M$. It is noted that the output of this procedure is a local $M$ versus $k$ prediction curve, which is size independent, because it is only a function of the assumed uniaxial stress-strain response. A 2D mesh refinement study is also included in Appendix I. The nonlocal $M$ versus $k$ prediction curve is obtained by scaling the local curvature estimate using Eq. (45) for four-point bending (see Appendix III). This implies that predicting size effect for ultimate strength is not feasible for the proposed nonlocal model.

The local $M$ versus $k$ response prediction can be transformed to a force versus midspan deflection curve by solving the boundary value problem for a simply supported Timoshenko beam under four-point bending (see Appendix III). Combining Eqs. (44) and (46), a local kinematic expression for the midspan deflection $\delta_m$ is obtained in terms of the curvature $k_m$, $\delta_m = 0.13611\, L^2\, k_m$, where $\delta_m$ is the midspan deflection corresponding to the curvature $k_m$. The nonlocal force versus midspan deflection curve is determined by imposing a similar kinematic relation between curvature and deflection, based on the gradient solution of the boundary problem [Eqs. (41) and (45)]. Unlike the local (classical) predictions, the nonlocal kinematic relation is affected by the internal length, $g$, which evolves with damage. Therefore, this kinematic relation is computed for the current value of $g$.

Regarding the evolution law for the gradient length, the study assumes an exponential expression of the form

$$g = g_0 e^{nD} \quad \text{for} \quad nD > 0 \tag{30}$$

where $g_0$ = initial internal length; $D$ = damage parameter; and $n$ = positive constant that defines the ratio of the gradient value $g_1$ (at $D = 1$) to the initial gradient internal length $g_0$ (at $D = 0$). Because the initial value of the gradient internal length is based on elasticity, there is only a single unknown parameter, $n$, to be determined based on experimental data in the inelastic region. It is worth noting that, according to Le Bellego et al. (2003), attempting to calibrate a gradient damage model assuming a constant internal length (independent of the damage level) resulted in a lack of objectivity when experimental data from geometrical similar notched beam specimens were considered. This could be partially remedied if an increasing value for the internal length is assumed with damage.

### Experimental Results

In this work, the experimental results of 13 geometrically similar ($L/h = 3$) plain concrete beam specimens with a maximum aggregate size, $d_{max} = 32$ mm, subjected to four-point bending (two equal loads $P/2$ applied at a distance $L/3$ from the beam supports) are considered (see Table 1). The tests were performed using a ±250 kN MTS hydraulic actuator under midspan deflection control to get the complete postpeak softening branch of the flexural response of the beams (see Fig. 4). The midspan deflection was the average of the measurements of two midspan DC displacement transducers (DCDTs), one on each side of the specimen, supported by a special aluminum frame attached to the beam ends above the supports (see Fig. 4). One of the two DCDTs was used as the controlling displacement sensor. Cylinder (150 × 300 mm) and cube specimens (150 × 150 × 150 mm) for the concrete mix were tested under uniaxial compression and indirect tension (splitting). Table 2 summarizes the experimental material properties. This is part of an extensive research program of four-point bending tests for six different types of cementitious mixes including cement mortar, plain concrete, and fiber-reinforced concrete, which is not the subject of this work.

**Table 1.** Experimental Program

| Specimen size | Nominal dimensions [$b \times h \times L$ (mm)] | Number of specimens tested[a] |
|---|---|---|
| S1 | 100 × 100 × 300 | 5 (5) |
| S2 | 150 × 150 × 450 | 5 (3) |
| S3 | 200 × 200 × 600 | 3 (2) |

Note: $b$ = width; $h$ = height; $L$= length.

[a]Number in parentheses denotes number of specimens with recorded postpeak softening branch.

The values of the uniaxial tension parameters $f_t$ and $\beta_t$ for the analysis were calibrated based on the measured peak load and corresponding deflection values in the four-point bending tests because uniaxial tension experiments were not performed, whereas the compression parameter $\beta_c$ was chosen to be consistent with the measured modulus of elasticity [see Eq. (28)]. The values for the uniaxial tension and compression parameters used for the analysis are $\beta_t = 6.5$, $f_t = 3.09$ MPa ($c = 12.313$), $\beta_c = 3.89$, and $\nu = 0.2$. The assumed value for $f_t$ appears to be consistent with the average splitting tensile strength ($f_t = 0.9 f_{sp}$) as Table 2 shows. The experimental results of the four-point bending tests for the initial stiffness showed a stiffer response than the classical elasticity predictions [Eq. (44)] for all sizes, and the initial gradient internal length value, $g_0$, corresponding to this deviation was estimated using Eq. (41). Based on the experimental results for the concrete mix considered, an initial value for the internal length of $g_0 = 8 \pm 4$ mm (mean ± SD) was found for all beam specimens considered. Furthermore, regarding the internal length evolution with damage [see Eq. (30)], a value of $n = 2$ appeared to give a good agreement with the experimental results, which corresponds to a mean internal length value for complete damage ($D = 1$) of $g_1 = 59$ mm.

The predicted value of $g_0$ can be physically interpreted as a measure of heterogeneity for the composite material. This heterogeneity is due to the presence of stiffer inclusions (aggregates) inside a matrix material and is governed by both the inclusion size and the elastic mismatch between the different phases of the composite (Triantafyllou and Giannakopoulos 2013a). During the inelastic deformation range, any initial heterogeneity is augmented because of the development of microcracks and hence the internal length should increase. However, the correlation between the initial microstructure of the composite and $g_0$, the justification for the

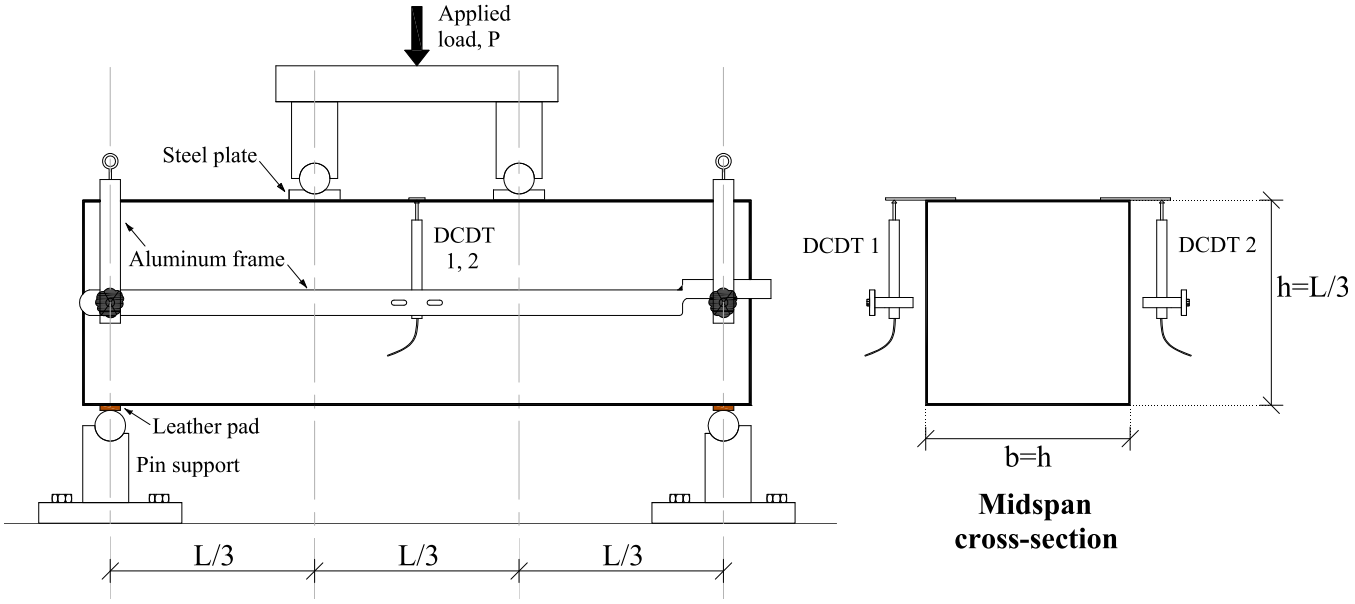


**Fig. 4.** Schematic of four-point bending experimental setup



J. Eng. Mech.

particular expression of Eq. (30), and the correlation between the internal length evolution law parameter, $n$, and other material properties (strength, brittleness, and fracture energy) cannot be discussed convincingly based only on the limited experimental results of a single concrete mix presented in this work. These important issues are currently under study. The aim of the present work is to provide experimental evidence for the finding that, based on the thermodynamic formulation, if $g = g(D)$, then $dg/dD \geq 0$, and with this respect the results of a single concrete mix appear to be sufficient.

Fig. 5 shows the measured flexural strength values, $\sigma_N = 3P/bh$, together with the numerical predictions. Note that no size effect is apparent in the strength values. Fig. 6 shows the experimental applied load $P$ versus midspan deflection diagrams including the unloading-reloading paths for the three sizes. Fig. 7 compares the model predictions with the experimental results for each size. It can be seen that an increasing internal length with damage improves the model predictions especially for large deflections, if all beam sizes are considered because the scatter in size S1 ($h/d_{\max} = 3.125$) is significant.

Furthermore, the measured softening branch appears steeper than the one predicted by the local model with increasing damage levels. This, in the context of gradient theory, can be explained only by an increasing internal length with damage. If the internal length is assumed constant with damage ($dg/dD = 0$), the local and nonlocal predictions are practically identical for all beam sizes.

Unloading and reloading was performed for most of the tests. The unloading path $(P, \delta)$ is depicted by an expression of the form, $P = \overline{P} - (1 - \overline{D})K_0(\overline{\delta} - \delta)$, where $\overline{P}$ and $\overline{\delta}$ are the values on the load versus midspan deflection curve where unloading starts, $\overline{D}$ is the average cross section damage parameter at the point $(\overline{P}, \overline{\delta})$ and $K_0$ is the initial stiffness for the uncracked concrete. Thus, the inelastic (plastic) midspan deflection upon complete unloading is

$$\delta_{pl} = \overline{\delta} - \overline{P}/(1 - \overline{D})K_0 \tag{31}$$

Fig. 8 plots the analytical normalized load at unloading with respect to the peak load, $\overline{P}/P_{\text{peak}}$, versus the normalized inelastic midspan deflection, $\delta_{pl}/\overline{\delta}$, together with the experimental results of the three specimen sizes. Fig. 8 shows both local and nonlocal predictions. The unloading estimates depend on the initial stiffness of the material ($K_0$) and the $\overline{P}$ versus $\overline{\delta}$ diagram model predictions. These

**Table 2.** Mechanical Properties of Concrete Mix

| Material properties | Measured values[a] |
|---|---|
| $f_{sp}$ (MPa) | 3.43 ± 0.1 (4) |
| $f_c$ (MPa) | 38.0 ± 3.6 (4) |
| $f_{\text{cube}}$ (MPa) | 54.7 ± 0.7 (3) |
| $E_0$ (GPa) | 34.0 ± 1 (3) |
| Strain, $\varepsilon_c$ | 0.0015 (3) |

[a]Number in parentheses denotes number of specimens considered.

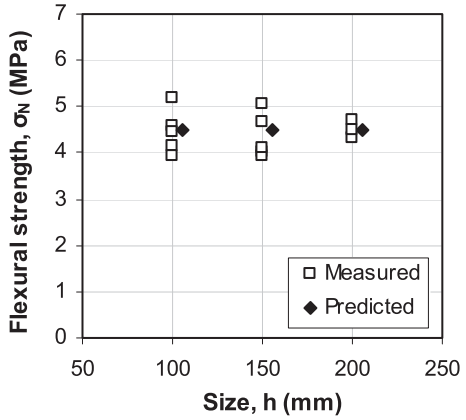


**Fig. 5.** Flexural strength $\sigma_N$ versus specimen size (experimental results and numerical predictions)

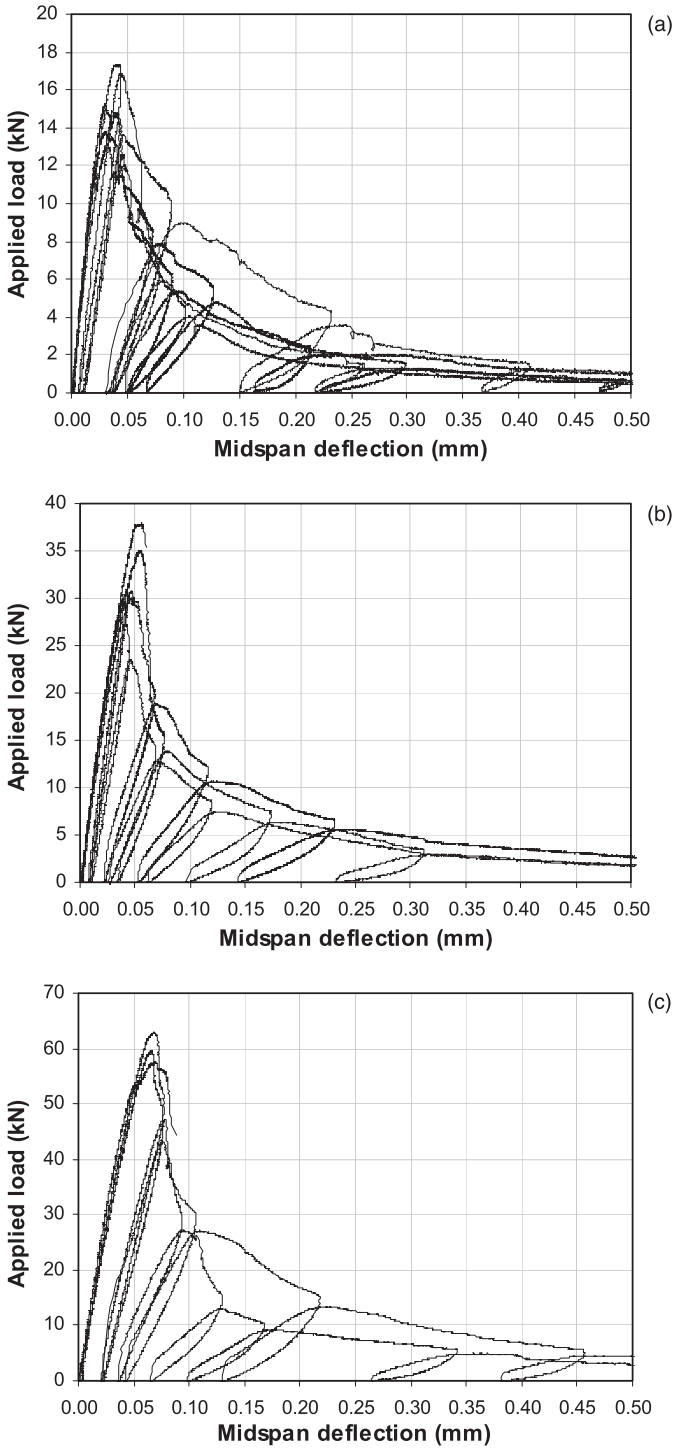


**Fig. 6.** Experimental applied load versus midspan deflection including unloading-reloading paths: (a) size S1; (b) size S2; (c) size S3

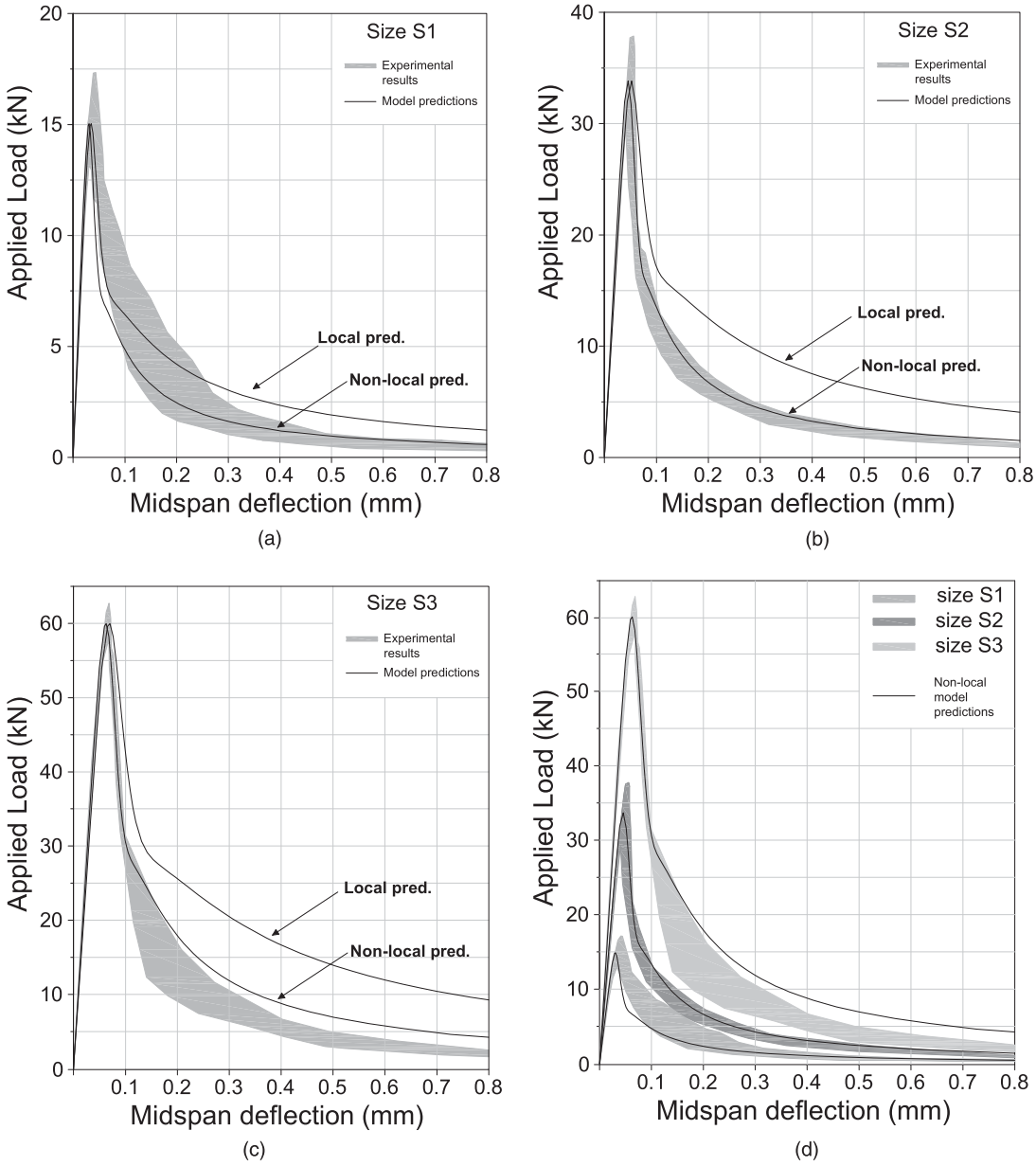


**Fig. 7.** Comparison of experimental results with numerical predictions: (a) size S1; (b) size S2; (c) size S3; (d) all sizes

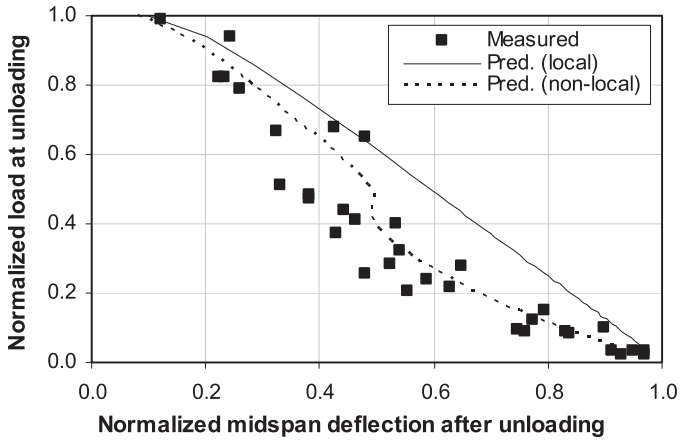


**Fig. 8.** Inelastic deformation after unloading (experimental results and numerical predictions)

estimates are closer to the experimental findings when the influence of the gradient internal length is considered, and this is reflected in the unloading values shown in Fig. 8.

## Conclusions

The current study proposes a strain gradient damage theory based on the influence of the stress gradient on Gibbs energy. It was shown that, if a microstructural internal length is related to the level of damage, this length should either increase with damage or remain constant. Furthermore, a simple continuous damage model was proposed for the case of four-point bending. Based on the present experimental results, the internal length evolution law is calibrated from standard tests on plain concrete and the resulting numerical nonlocal predictions are in good agreement with the experimental results. Furthermore, the deviation of the local model predictions (classical elasticity) from the experimental results increases with increasing beam size. This size effect in the inelastic beam response

(softening) is better captured by the nonlocal model by using the same internal length evolution law for all sizes.

## Appendix I. Objectivity of the Present Model Predictions

The total strain $\boldsymbol{\varepsilon}$, is related to the total displacement $\mathbf{u}[\varepsilon_{ij} = (\partial u_i/\partial x_j + \partial u_j/\partial x_i)/2]$, where $\varepsilon_{ij}$ is the gradient-enriched strain. The damage rules of Eq. (9) provide the stiffness evolution as functions of the Cauchy stress $\boldsymbol{\tau}$, which in turn relates to the total strain as $\boldsymbol{\tau} = \mathbf{C}^{-1}:\boldsymbol{\varepsilon}$. For a 1D case, the equilibrium equation $(\partial\sigma/\partial x = 0)$ within the framework of the proposed gradient model becomes

$$\frac{\partial\sigma}{\partial\varepsilon}\frac{\partial\varepsilon}{\partial x}+\frac{\partial\sigma}{\partial\varepsilon_{,xx}}\frac{\partial\varepsilon_{,xx}}{\partial x}=\frac{\partial\sigma}{\partial\varepsilon}\frac{\partial^2 u}{\partial x^2}+\frac{\partial\sigma}{\partial\varepsilon_{,xx}}\frac{\partial^4 u}{\partial x^4}=0 \tag{32}$$

The constitutive law assumed in this work can be expressed as

$$\sigma(\varepsilon,\varepsilon_{,xx}) = [1-D(\varepsilon)]E(\varepsilon - g^2\varepsilon_{,xx}) \tag{33}$$

where $D(\varepsilon) = [\varepsilon_u(\varepsilon-\varepsilon_i)]/[\varepsilon(\varepsilon_u-\varepsilon_i)]$ = damage loading function for uniaxial tension ($\varepsilon_i$ = strain signifying end of elastic behavior; $\varepsilon_u$ = strain signifying complete damage; and $\varepsilon$ = applied uniform axial tensile strain equal to $\varepsilon_{t0}$).

Assuming a harmonic perturbation for the displacement, $u = A\cos(\varphi x)$, where $\varphi$ = wave number and $A$ = amplitude, Eq. (32) becomes

$$\frac{E\varepsilon_i}{\varepsilon_u-\varepsilon_i}\left[\left(\frac{\varepsilon_u}{\varepsilon_{t0}}-1\right)g^2\varphi^2-1\right]=0 \tag{34}$$

It can be seen that Eq. (34) yields a real wave number with a critical value of $\varphi_{\text{crit}} = (1/g)\sqrt{\varepsilon_{t0}/(\varepsilon_u-\varepsilon_{t0})}$, which is identical to that in Rodriguez-Ferran et al. (2011). Such a result renders a nonlocal model suitable for regularization if employed in a FEM analysis.

Fig. 9 shows a 2D mesh refinement study of the presented model for the beam specimen size S3 at a load level of $0.84P_{\text{peak}}$ in the postpeak softening branch. Based on the 1D-discretized midspan cross section (strips of depth $dz$), this load level of $0.84P_{\text{peak}}$ corresponds to the first detection of a damage value of $D = 0.95$. Three sizes for an $xyz$ grid are used with a width of $b = 200$ mm: (1) $20\times200\times20$ mm, (2) $10\times200\times10$ mm, and (3) $5\times200\times5$ mm. It can be seen that mesh-independent damage predictions are obtained along the beam's length. The calculated damage levels are the same for both local and nonlocal $\overline{P}$ versus $\overline{\delta}$ predictions [see Fig. 7(c)]. A damage value of $D \geq 0.95$, corresponding practically to zero stress transfer capability, may signify major crack development. The model's prediction that a major crack forms at a load level of $0.84P_{\text{peak}}$ in the postpeak softening branch is in agreement with acoustic emission findings for concrete beams under flexure (Zhu et al. 2010) and uniaxial tension (Li and Shah

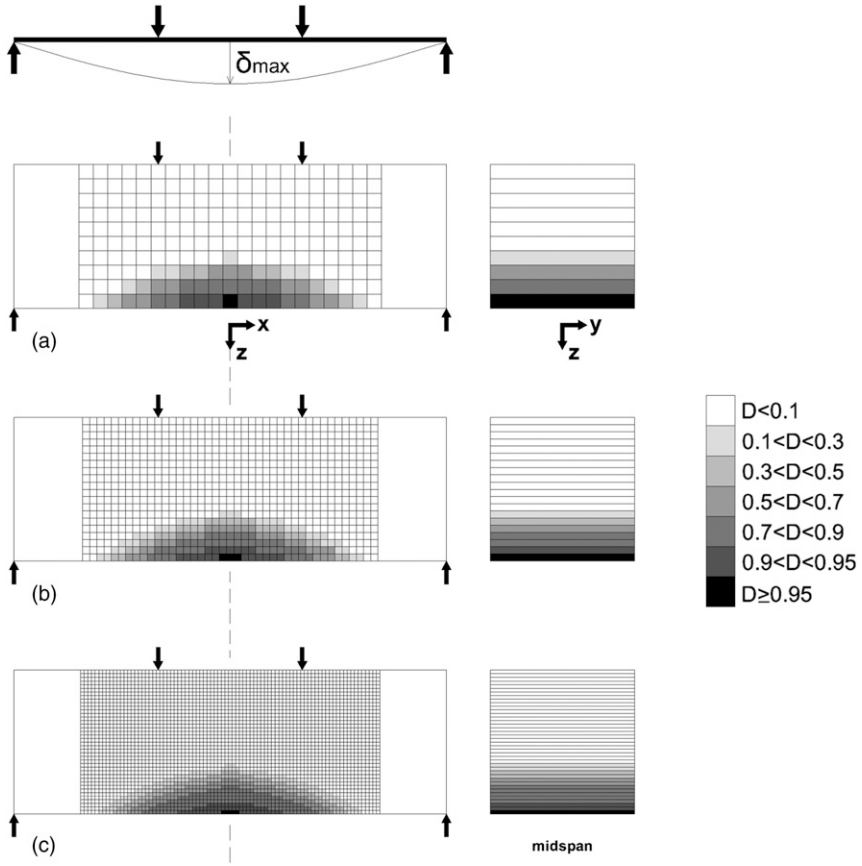


**Fig. 9.** Numerical damage level predictions of 2D mesh refinement study of proposed model for specimen size S3 ($200\times200\times600$ mm) at $0.84P_{\text{peak}}$ in the postpeak softening branch with grids (a) $20\times20$ mm; (b) $10\times10$ mm; (c) $5\times5$ mm

1994). Also, it is noted that a nonzero midspan damage value $\overline{D}$ is computed at $0.74P_{\text{peak}}$ in the ascending branch of response. A damage value of $D > 0$, signifying softening in uniaxial tension, can be associated with microcracking activity. Acoustic emission experiments on notched and unnotched concrete beam specimens tested under flexure have shown that microcracking activity becomes detectable before the peak applied load is reached and at load levels between 70 and 80% of the peak load (Chen and Liu 2004; Zhu et al. 2010).

## Appendix II. Energy Dissipation during Microcrack Extension

Two 2D isotropic cases are considered, as Fig. 10 shows. Fig. 10(a) depicts a microcrack subjected to a uniform tensile stress, and Fig. 10(b) depicts a microcrack under a stress gradient. The model predictions in this study do not assume interaction between the microcracks and elastic anisotropy.

For a crack of length 2a, loaded by a uniform tensile stress, $\tau$, as shown in Fig. 10(a), the stress intensity factors for Modes I and II, neglecting Mode III, are (Tada et al. 1973): $K_{\text{I}} = \tau\sqrt{\pi a}\sin^2\phi$ and $K_{\text{II}} = \tau\sqrt{\pi a}\sin\phi\cos\phi$, and the energy release rate is $G = (K_{\text{I}}^2 + K_{\text{II}}^2)/E^*$, where $E^* = E$ for plane stress, $E^* = E/(1-\nu^2)$ for plane strain, $E$ is the elastic modulus, and $\nu$ is Poisson's ratio.

The crack can occur at an arbitrary angle value $\phi$ assuming the same probability of occurrence at all possible angle values. Therefore, the 2D average energy release rate per unit length of microcrack is

$$\left\langle \frac{dG}{da} \right\rangle = \frac{\pi\tau^2}{E^*}\frac{1}{\pi}\int_{-\pi/2}^{\pi/2}\sin^2(\phi)d\phi = \frac{\pi\tau^2}{2E^*} \tag{35}$$

where $\langle\,\rangle$ denotes the average of the quantity enclosed in the brackets.

For a crack of length $2a$, under pure bending, as shown in Fig. 10(b), the stress intensity factors for Modes I and II (Bowie and Freese 1976) are $K_{\text{I}} = (d\tau/dy)(2a/3)^{3/2}\sin^3(\phi)$ and $K_{\text{II}} = (d\tau/dy)(2a/3)^{3/2}\sin^2(\phi)\cos(\phi)$. The average 2D energy release rate per unit length of a microcrack for all possible angles is

$$\left\langle \frac{dG}{da} \right\rangle = \frac{2}{E^*}\left(\frac{d\tau}{dy}\right)^2\left(\frac{2a}{3}\right)^2\frac{1}{\pi}\int_{-\pi/2}^{\pi/2}\sin^4(\phi)d\phi = \frac{1}{3E^*}\left(\frac{d\tau}{dy}a\right)^2 \tag{36}$$

Stallybrass (1970) considered crack propagation under a nonuniform stress field, and Huang and Detournay (2013) used it to improve the accuracy of crack propagation predictions in quasi-brittle materials subjected to an indentation.

Damage can be introduced in different ways depending on the damage parameter definition. The damage parameter $\mu$ is associated with the damage parameter $D$ through Eq. (25), and differentiating both parts yields

$$d(E^*\mu) = \frac{dD}{(1-D)^2} \tag{37}$$

Accounting for the effect of damage on the Young's modulus, the free energy density required to form microcracks should be

$$A^c = \frac{1}{1-D}\left\langle \frac{dG}{da} \right\rangle \tag{38}$$

Thus, the energy dissipated during microcrack propagation is

$$\frac{dA^c}{dD} = \frac{1}{(1-D)^2}\left\langle \frac{dG}{da} \right\rangle \tag{39}$$

Using Eq. (39), the energy dissipated during crack propagation can be expressed with respect to $\mu$ as

$$\frac{dA^c}{d\mu} = (1-D)^2E^*\frac{dA^c}{dD} = E^*\left\langle \frac{dG}{da} \right\rangle = \frac{\pi}{2}\tau^2 + \frac{1}{3}\left(\frac{d\tau}{dy}a\right)^2 \tag{40}$$

Obviously, the crack length, $a$, and the internal length, $g$, are functions of the damage parameter. Therefore, $g = g(\mu) = \psi(a)$ and $a = \psi^{-1}(g) = \xi(\mu)$. It should be noted that a stress gradient cannot induce crack opening under a compressive mode (see Fig. 10). The stress gradient is essentially a bending moment and thus, one half of the crack length will be under a compressive stress and the other half under a tensile stress. The latter corresponds to a tensile opening mode $I_T$, whereas the former corresponds to Fig. 2(c), which does not induce crack extension.

## Appendix III. Midspan Deflection for Four-Point Bending Based on Gradient Elasticity

The boundary value problem for a dipolar elastic Timoshenko simply supported beam has been solved in closed-form by Triantafyllou and Giannakopoulos (2013b) and only the relevant work is included here.

The expression for the midspan deflection of a simply supported beam with an orthogonal cross section subjected to two equal concentrated loads, $P/2$, at a distance $L/3$ from the supports is

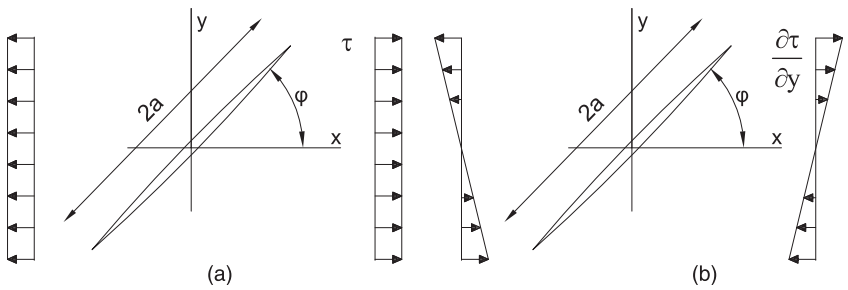


**Fig. 10.** Crack of length 2a under (a) uniaxial tension; (b) pure bending

$$\delta = \frac{23PL^3}{1{,}296\overline{E}I}\left(\frac{\ell}{g}\right)^2\left[(1-f_b)+\frac{216}{115}\left(\frac{h}{L}\right)^2\left(\frac{g}{\ell}\right)^2\left(\frac{1-\nu}{1-2\nu}\right)(1-f_{sh})\right] \tag{41}$$

where $P$ = applied load by the actuator; $\overline{E} = [(1-\nu)/(1+\nu)(1-2\nu)]E_0$; $E_0$ = Young's modulus of elasticity; $\ell = g\sqrt{1/[1+(A/I)g^2]}$, a shear gradient internal length; and $f_b, f_{sh}$ = nondimensional functions of the internal length $g$ [see the following equations, Eqs. (42) and (43)]

$$f_{sh} = -\frac{g}{L}\frac{\left[e^{11L/6g}\left(6\frac{g}{L}-2\right)+3e^{4L/3g}-e^{2L/g}+2e^{L/6g}\left(3\frac{g}{L}+1\right)-2e^{7L/6g}\left(3\frac{g}{L}+1\right)+e^{5L/6g}\left(2-6\frac{g}{L}\right)+1-3e^{2L/3g}\right]}{\left[2\left(1-e^{2L/g}\right)\frac{g}{L}+\left(1+e^{2L/3g}+e^{4L/3g}+e^{2L/g}\right)\right]} \tag{42}$$

$$f_b = \frac{\alpha_1}{\Delta_1}+\frac{\alpha_2+\alpha_3+\alpha_4+\alpha_5+\alpha_6+\alpha_7}{\Delta} \tag{43}$$

where

$$\alpha_1 = 32\left(\frac{g}{L}\right)\left(1-e^{L/6g}-e^{5L/6g}+e^{7L/6g}+e^{11L/6g}-e^{2L/g}\right)$$

$$\alpha_2 = 96\left(\frac{\ell}{L}\right)\left(1+e^{2L/3g}+e^{4L/3g}+e^{2L/g}\right)\left(-1+e^{2L/\ell}\right)$$

$$\alpha_3 = 96\left(\frac{\ell}{L}\right)\left(\frac{g}{L}\right)\left(1-e^{L/g}\right)\left(e^{2L/3g}-1\right)\left[3-e^{L/6g}-e^{5L/6g}+3e^{L/g}-4e^{L/6(5/g+4/\ell)}-e^{L/6(5/g+8/\ell)}+6e^{L/g+2L/3\ell}+3e^{L/g+4L/3\ell}+6e^{2L/3\ell}+3e^{4L/3\ell}-4e^{L(4g+\ell)/6g\ell}-e^{L(8g+\ell)/6g\ell}\right]$$

$$\alpha_4 = 288e^{L/6g}\left(\frac{g}{L}\right)\left(\frac{\ell}{L}\right)^2\left(e^{L/g}-1\right)\left[2+2e^{L/6g}-4e^{L/6(1/g+1/\ell)}+2e^{L(1/g+1/\ell)}+4e^{L/6(5/g+3/\ell)}+4e^{L/6(5/g+7/\ell)}-4e^{L/6(5/g+9/\ell)}-7e^{L/g+L/2\ell}+2e^{L/g+2L/3\ell}-7e^{L/g+7L/6\ell}+2e^{L/g+5L/3\ell}-7e^{L/2\ell}+2e^{2L/3\ell}+2e^{L/\ell}-7e^{7L/6\ell}+2e^{5L/3\ell}+4e^{L(3g+\ell)/6g\ell}+4e^{L(7g+\ell)/6g\ell}-4e^{L(9g+\ell)/6g\ell}-4e^{L(g+5\ell)/6g\ell}\right]$$

$$\alpha_5 = 144\left(\frac{\ell}{L}\right)^2\left[3e^{2L/3(3/g+1/\ell)}-2e^{L/6(4/g+1/\ell)}+4e^{L/3(4/g+1/\ell)}+4e^{L/3(6/g+1/\ell)}+4e^{L/3(2/g+5/\ell)}-2e^{L/6(4/g+5/\ell)}+4e^{L/3(4/g+5/\ell)}-2e^{L/6(8/g+5/\ell)}-2e^{L/6(4/g+7/\ell)}-2e^{L/6(8/g+7/\ell)}-2e^{L/6(4/g+11/\ell)}-2e^{L/6(8/g+11/\ell)}-2e^{2L/g+L/6\ell}-2e^{2L/g+5L/6\ell}-2e^{2L/g+7L/6\ell}+3e^{2L/g+4L/3\ell}+4e^{2L/g+5L/3\ell}-2e^{2L/g+11L/6\ell}-2e^{L/6\ell}+4e^{L/3\ell}+3e^{2L/3\ell}-2e^{5L/6\ell}-2e^{7L/6\ell}+3e^{4L/3\ell}+4e^{5L/3\ell}-2e^{11L/6\ell}+3e^{2L(g+\ell)/3g\ell}+3e^{4L(g+\ell)/3g\ell}+3e^{2L(2g+\ell)/3g\ell}+4e^{L(g+2\ell)/3g\ell}+3e^{2L(g+2\ell)/3g\ell}-2e^{L(g+8\ell)/6g\ell}\right]$$

$$\alpha_6 = 432\left(\frac{\ell}{L}\right)^3\left(\frac{g}{L}\right)\left[2+e^{L/6g}+e^{5L/6g}-e^{7L/6g}-e^{11L/6g}-2e^{2L/g}+2e^{2(L/g+L/\ell)}-2e^{2/3(3L/g+L/\ell)}+2e^{1/2(4L/g+L/\ell)}-3e^{1/6(5L/g+4L/\ell)}+3e^{1/6(7L/g+4L/\ell)}+3e^{1/6(11L/g+4L/\ell)}+3e^{1/6(5L/g+8L/\ell)}-3e^{1/6(7L/g+8L/\ell)}-3e^{1/6(11L/g+8L/\ell)}-2e^{(2L/g+5L/6\ell)}+2e^{(2L/g+7L/6\ell)}+2e^{(2L/g+4L/3\ell)}-2e^{(2L/g+3L/2\ell)}-e^{(L/6g+2L/\ell)}-e^{(5L/6g+2L/\ell)}+e^{(7L/6g+2L/\ell)}+e^{(11L/6g+2L/\ell)}-2e^{L/2\ell}+2e^{2L/3\ell}+2e^{5L/6\ell}-2e^{7L/6\ell}-2e^{4L/3\ell}+2e^{3L/2\ell}-2e^{2L/\ell}-3e^{1/6(L/g+4L/\ell)}+3e^{1/6(L/g+8L/\ell)}\right]$$

$$\alpha_7 = 216\left(\frac{\ell}{L}\right)^3\left[3+3e^{2L/3g}+3e^{4L/3g}+3e^{2L/g}-e^{2/3(3L/g+L/\ell)}-2e^{1/2(4L/g+L/\ell)}-3e^{2/3(L/g+3L/\ell)}-2e^{1/6(4L/g+3L/\ell)}-2e^{1/6(8L/g+3L/\ell)}+2e^{1/6(4L/g+5L/\ell)}+2e^{1/6(8L/g+5L/\ell)}-2e^{1/6(4L/g+7L/\ell)}-2e^{1/6(8L/g+7L/\ell)}+2e^{1/6(4L/g+9L/\ell)}+2e^{(8L/g+9L/6\ell)}+2e^{(2L/g+5L/6\ell)}-2e^{(2L/g+7L/6\ell)}+2e^{(2L/g+4L/3\ell)}+2e^{(2L/g+3L/2\ell)}-3e^{(4L/3g+2L/\ell)}-2e^{L/2\ell}-2e^{2L/3\ell}+2e^{5L/6\ell}-2e^{7L/6\ell}+e^{4L/3\ell}+2e^{3L/2\ell}-3e^{2L/\ell}-e^{2/3(L/g+L/\ell)}+e^{4/3(L/g+L/\ell)}-3e^{2(L/g+L/\ell)}+e^{2/3(L/g+2L/\ell)}-e^{2/3(2L/g+L/\ell)}\right]$$

$$\Delta_1 = 23\left[\left(1+e^{2L/3g}+e^{4L/3g}+e^{2L/g}\right)+2\left(\frac{g}{L}\right)\left(1-e^{2L/g}\right)\right],$$

$$\Delta = \left(1+e^{2L/3\ell}+e^{4L/3\ell}+e^{2L/\ell}\right)\Delta_1$$

Note that Eq. (41) accounts for the effect of Poisson's ratio on the Young's modulus. In the absence of gradient, i.e., $g = 0$ ($\ell/g = 1$), Eq. (41) reduces to the classical elasticity solution

$$\delta = \frac{23PL^3}{1{,}296\bar{E}I}\left[1 + \frac{216}{115}\left(\frac{h}{L}\right)^2\left(\frac{1-\nu}{1-2\nu}\right)\right] \tag{44}$$

The expression for the normal axial strain of the beam at midspan at a distance $z$ from the neutral axis is given by

$$\varepsilon_{xx} = kz = \frac{PL}{6\bar{E}I}\left(\frac{\ell}{g}\right)^2 \times \left[1 - \frac{2e^{L/6\ell}\left(2 + 2e^{L/\ell} + 3\frac{\ell}{L}e^{L/3\ell} - 3\frac{\ell}{L}e^{2L/3\ell}\right)}{3\left(1 + 4e^{4L/3\ell}\right)}\right] z \tag{45}$$

where $k$ = beam's curvature; and $-h/2 \le z \le h/2$. Of course, in the absence of gradient, i.e., $g = 0$, Eq. (45) reduces to the classical expression for the axial strains

$$\varepsilon_{xx\_cl} = k_{cl}z = \frac{PL}{6\bar{E}I}z \tag{46}$$

## Acknowledgments

This work is part of the Herakleitos II project of the Greek Ministry of National Education for basic research on the size effect phenomena of concrete and is cofinanced by the European Union [European Social Fund (ESF)] and Greek National funds through the Education and Lifelong Learning operational program of the National Strategic Reference Framework (NSRF). The experimental work presented here was performed in the Reinforced Concrete Technology and Structures Laboratory of the Civil Engineering Department at the University of Thessaly.

## References

Addessi, D., Marfia, S., and Sacco, E. (2002). "A plastic nonlocal damage model." *Comput. Methods Appl. Mech. Eng.*, 191(13–14), 1291–1310.

Aggelis, D. G., and Shiotani, T. (2007). "Experimental study of surface wave propagation in strongly heterogeneous media." *J. Acoust. Soc. Am.*, 122(5), EL151–EL157.

Aggelis, D. G., and Shiotani, T. (2008). "Surface wave dispersion in cement-based media: Inclusion size effect." *NDT&E Int.*, 41(5), 319–325.

Bažant, Z. P. (1991). "Why continuum damage is nonlocal: Micromechanics arguments." *J. Eng. Mech.*, 10.1061/(ASCE)0733-9399(1991)117:5(1070), 1070–1087.

Bažant, Z. P., and Planas, J. (1997). *Fracture and size effect in concrete and other quasibrittle materials*, CRC Press, Boca Raton, FL.

Benvenuti, E., Borino, G., and Tralli, A. (2002). "A thermodynamically consistent nonlocal formulation for damaging materials." *Eur. J. Mech. A, Solids*, 21(4), 535–553.

Borino, G., Failla, B., and Parrinello, F. (2003). "A symmetric nonlocal damage theory." *Int. J. Solids Struct.*, 40(13–14), 3621–3645.

Bowie, O. L., and Freese, C. E. (1976). "On the 'overlapping' problem in crack analysis." *Eng. Fract. Mech.*, 8(2), 373–379.

Budiansky, B., and O'Connell, R. J. (1976). "Elastic moduli of a cracked solid." *Int. J. Solids Struct.*, 12(2), 81–97.

Bui, Q. V. (2010). "Initiation of damage with implicit gradient-enhanced damage models." *Int. J. Solids Struct.*, 47(18–19), 2425–2435.

Chen, B., and Liu, J. (2004). "Effect of aggregate on the fracture behavior of high strength concrete." *Construct. Build. Mater.*, 18(8), 585–590.

Chen, L., Shao, J. F., Zhu, Q. Z., and Duveau, G. (2012). "Induced anisotropic damage and plasticity in initially anisotropic sedimentary rocks." *Int. J. Rock Mech. Min. Sci.*, 51(Apr), 13–23.

Comi, C. (1999). "Computational modelling of gradient-enhanced damage in quasi-brittle materials." *Mech. Cohesive-Frictional Mater.*, 4(1), 17–36.

de Borst, R., and Gutierrez, M. A. (1999). "A unified framework for concrete damage and fracture models including size effects." *Int. J. Fract.*, 95(1–4), 261–277.

Desmorat, R., Gatuingt, F., and Ragueneau, F. (2010). "Nonstandard thermodynamics framework for robust computations with induced anisotropic damage." *Int. J. Damage Mech.*, 19(1), 53–73.

Fremond, M., and Nedjar, B. (1996). "Damage, gradient of damage and principle of virtual power." *Int. J. Solids Struct.*, 33(8), 1083–1103.

Geers, M. G. M., de Borst, R., Brekelmans, W. A. M., and Peerlings, R. H. J. (1998). "Strain-based transient-gradient damage model for failure analyses." *Comput. Methods Appl. Mech. Eng.*, 160(1–2), 133–153.

Georgiadis, H. G., and Grentzelou, C. G. (2006). "Energy theorems and the $J$-integral in dipolar gradient elasticity." *Int. J. Solids Struct.*, 43(18–19), 5690–5712.

Georgiadis, H. G., Vardoulakis, I., and Velgaki, E. G. (2004). "Dispersive Rayleigh-wave propagation in microstructured solids characterized by dipolar gradient elasticity." *J. Elast.*, 74(1), 17–45.

Horii, H., and Nemat-Nasser, S. (1983). "Overall moduli of solids with microcracks: Load-induced anisotropy." *J. Mech. Phys. Solids*, 31(2), 155–171.

Huang, H., and Detournay, E. (2013). "Discrete element modeling of tool-rock interaction II: Rock indentation." *Int. J. Numer. Anal. Methods Geomech.*, 37(13), 1930–1947.

Kachanov, M. (1980). "Continuum model of medium with cracks." *J. Engrg. Mech. Div.*, 106(5), 1039–1051.

Le Bellego, C., Dube, J. F., Pijaudier-Cabot, G., and Gerard, B. (2003). "Calibration of nonlocal damage model from size effect tests." *Eur. J. Mech. A, Solids*, 22(1), 33–46.

Li, F., and Li, Z. (2000). "Acoustic emission monitoring of fracture of fiber-reinforced concrete in tension." *ACI Mater. J.*, 97(6), 629–636.

Li, J. (2011). "A micromechanics-based strain gradient damage model for fracture prediction of brittle materials—Part I: Homogenization methodology and constitutive relations." *Int. J. Solids Struct.*, 48(24), 3336–3345.

Li, J., Pham, T., Abdelmoula, R., Song, F., and Jiang, C. P. (2011). "A micromechanics-based strain gradient damage model for fracture prediction of brittle materials—Part II: Damage modeling and numerical simulations." *Int. J. Solids Struct.*, 48(24), 3346–3358.

Li, Z., and Shah, S. P. (1994). "Localization of microcracking in concrete under uniaxial tension." *ACI Mater. J.*, 91(4), 372–381.

Mazars, J., and Pijaudier-Cabot, G. (1989). "Continuum damage theory—Application to concrete." *J. Eng. Mech.*, 10.1061/(ASCE)0733-9399(1989)115:2(345), 345–365.

Mazars, J., Pijaudier-Cabot, G., and Saouridis, C. (1991). "Size effect and continuous damage in cementitious materials." *Int. J. Fract.*, 51(2), 159–173.

Mindlin, R. D. (1964). "Micro-structure in linear elasticity." *Arch. Ration. Mech. Anal.*, 16(1), 51–78.

Murakami, S., and Kamiya, K. (1997). "Constitutive and damage evolution equations of elastic-brittle materials based on irreversible thermodynamics." *Int. J. Mech. Sci.*, 39(4), 473–486.

Nguyen, G. D. (2008). "A thermodynamic approach to non-local damage modelling of concrete." *Int. J. Solids Struct.*, 45(7–8), 1918–1934.

Ortiz, M. (1985). "A constitutive theory for the inelastic behavior of concrete." *Mech. Mater.*, 4(1), 67–93.

Peerlings, R. H. J., de Borst, R., Brekelmans, A. M., and de Vree, H. H. P. (1996). "Gradient enhanced damage for quasi-brittle materials." *Int. J. Numer. Methods Eng.*, 39(19), 3391–3403.

Peerlings, R. H. J., Geers, M. G. D., de Borst, R., and Brekelmans, W. A. M. (2001). "A critical comparison of nonlocal and gradient-enhanced softening continua." *Int. J. Solids Struct.*, 38(44–45), 7723–7746.

Pijaudier-Cabot, G., and Bažant, Z. P. (1987). "Nonlocal damage theory." *J. Eng. Mech.*, 10.1061/(ASCE)0733-9399(1987)113:10(1512), 1512–1533.

Pijaudier-Cabot, G., Haidar, K., and Dube, J. F. (2004). "Non-local damage model with evolving internal length." *Int. J. Numer. Anal. Methods Geomech.*, 28(7–8), 633–652.

Poh, L. H., and Swaddiwudhipong, S. (2009). "Gradient-enhanced softening material models." *Int. J. Plast.*, 25(11), 2094–2121.
Popovics, S. A. (1973). "A numerical approach to the complete stress-strain curve of concrete." *Cement Concr. Res.*, 3(5), 583–599.
Rodriguez-Ferran, A., Bennett, T., Askes, H., and Tamayo-Mas, E. (2011). "A general framework for softening regularisation based on gradient elasticity." *Int. J. Solids Struct.*, 48(9), 1382–1394.
Simone, A., Askes, H., and Sluys, L. (2004). "Incorrect initiation and propagation of failure in non-local and gradient-enhanced media." *Int. J. Solids Struct.*, 41(2), 351–363.
Stallybrass, M. P. (1970). "A crack perpendicular to an elastic half-plane." *Int. J. Eng. Sci.*, 8(5), 351–353.
Stamoulis, K., and Giannakopoulos, A. E. (2010). "A second gradient elasto-plastic model for fatigue of small-scale metal components." *Int. J. Struct. Int.*, 1(3), 193–208.
Tada, H., Paris, P. C., and Irwin, G. R. (1973). *The stress analysis of cracks handbook*, Del Research Corporation, Hellertown, PA.
Triantafyllou, A., and Giannakopoulos, A. E. (2013a). "Derivation of strain gradient length via homogenization of heterogeneous elastic materials." *Mech. Mater.*, 56(Jan), 23–37.
Triantafyllou, A., and Giannakopoulos, A. E. (2013b). "Structural analysis using a dipolar elastic Timoshenko beam." *Eur. J. Mech. A, Solids*, 39(May–Jun), 218–228.
Voyiadjis, Z. G., and Abu Al-Rub, R. K. (2005). "Gradient plasticity theory with a variable length scale parameter." *Int. J. Solids Struct.*, 42(14), 3998–4029.
Wu, J. Y., Li, J., and Faria, R. (2006). "An energy release rate-based plastic-damage model for concrete." *Int. J. Solids Struct.*, 43(3–4), 583–612.
Zhu, W. C., Zhao, X. D., Kang, Y. M., Wei, C. H., and Tian, J. (2010). "Numerical simulation on the acoustic emission activities of concrete." *Mater. Struct.*, 43(5), 633–650.